PHYSICAL REVIEW B VOLUME 40, NUMBER 12 15 OCTOBER 1989-II

Electronic structures of zero-dimensional quantum wells

Jian-Bai Xia
China Center of Advanced Sciences and Technology (World Laboratory), Beijing, China
and Institute of Semiconductors, Chinese Academy of Sciences, P.O. Box 912, Beijing 100083, China

(Received 28 November 1988; revised manuscript received 22 May 1989)

The electronic structures of zero-dimensional quantum wells are studied with a spherical model in the framework of the effective-mass theory. The mixing effect of the heavy and light holes is taken into account, and the symmetry classification and the energy levels of hole states are obtained. The energies of the donor and acceptor states are calculated. The difference between the shallow-impurity states and the eigenstates for the small semiconductor sphere disappears. The selection rules for the optical transition between the conduction- and valence-band states are obtained. The $\Delta n = 0$ selection rule is not followed strictly because of the mixing of the L- and $(L+2)$-orbital wave functions in the wave functions of the hole states. The exciton binding energies are calculated for the small GaAs spheres. The energy levels of the ZnSe spheres are given as functions of the radius and compared with the experiments.

I. INTRODUCTION

In recent years semiconductor superlattices have developed from two dimensional (2D) to one dimensional, and even zero dimensional. Since the electronic movement in the zero-dimensional superlattices (ZDS's) is confined in all three directions, it is expected that there will appear more obvious quantum size effects, for example they will have discrete quantum energy levels just as in large molecules and the energy levels will be strongly dependent on the size of the ZDS. At present there have been some measurements of the optical and electric properties of ZDS's.[1-5] There also have been attempts to use ZDS's in microelectronics as memory devices by constructing a very regular array of ultrafine particles on silicon.[6] In the field of chemistry, small semiconductor crystallites are used as catalysts and photosensitizers.[7-10] In the case of CdS and other cyrstallites, moderate changes in electronic absorption and resonance Raman excitation spectra have been reported.[11,12]

There have been many reports on the electronic structures of the two-dimensional superlattices, while reports on lower-dimensional superlattices are still few. Xia and Huang[13] and Brum *et al.*[14] calculated the electronic and hole subband structures of one-dimensional superlattices. Brus *et al.*[15,12] calculated the energy levels and exciton energies of small semiconductor crystalline spheres by the effective-mass approximation. In Ref. 12 they pointed out that for the hole the Baldereschi and Lipari Hamiltonian[16] should be used, and the mixing between the S and D states, heavy- and light-hole states, and spin-orbit splitting states may be important. Kayanuma[17] and Nair *et al.*[18] calculated the lowest energies of the electron-hole pair states in the simple-parabolic-band approximation by the variation and perturbation methods. In this paper we shall use a spherical quantum-well model to simulate the ZDS's and use the effective-mass envelope-function method to calculate the electronic structures. For electrons we use the simple-parabolic-band model, while for holes we use the Baldereschi and Lipari[19] spherical-model Hamiltonian in the limit of strong spin-orbit coupling between the valence bands. Section II gives the calculation method. Section III gives the results on electronic and hole energy levels. Section IV gives the donor and acceptor energy levels. Section V deals with optical transition probabilities and selection rules. Section VI presents calculation of the exciton energies. Section VII gives the energy levels of the small ZnSe sphere as functions of the radius, and compares them with the experiments.

II. CALCULATION METHOD

We assume a spherical quantum-well model: the electron and hole are confined in a spherical, infinite potential well. In the spherical coordinate system the equation of the radial function $f(r)$ for the electron is

$$\left[-\frac{d^2}{dr^2}-\frac{2}{r}\frac{d}{dr}+\frac{l(l+1)}{r^2}\right]f(r)=Ef(r)\ , \tag{1}$$

where $f(r)$ satisfies the boundary condition,

$$f(R)=0\ . \tag{2}$$

R is the radius of the sphere. Equation (1) has solutions,

$$f_{nl}(r)=A_{nl}j_l(K_{nl}r)\ , \tag{3}$$

where n and l are the main and angular quantum numbers, respectively, $j_l(\rho)$ is the spherical Bessel function,[20] and A_{nl} is the normalization constant. K_{nl} is determined by the zeros of $j_l(\rho)$,

$$K_{nl}R=\rho_{nl}\ . \tag{4}$$

In this paper, we use the effective Bohr radius

$$a_0^*=\frac{\hbar^2\epsilon_0}{m^*e^2} \tag{5}$$

and the effective Rydberg

$$R_0^* = \frac{m^* e^4}{2\hbar^2 \epsilon_0^2} \tag{6}$$

as units of length and energy, respectively. ϵ_0 is the dielectric constant, and m^* is the effective mass. For electrons $m^* = m_e^*$, for holes $m^* = 1/\gamma_1$.

On the assumption of the isotropy of the hole energy bands ($\gamma_2 = \gamma_3$), the effective-mass Hamiltonian of the hole is[19]

$$H = p^2 - \frac{\mu}{9}(P^{(2)} \cdot J^{(2)}) , \tag{7}$$

where $P^{(2)}$ and $J^{(2)}$ are the second-order irreducible tensor operators of the momentum and angular momentum corresponding to spin $\frac{3}{2}$, respectively,

$$\mu = \frac{2\gamma_2}{\gamma_1} , \tag{8}$$

and γ_1, γ_2, and γ_3 are the Luttinger effective-mass parameters.[21] From Eq. (7) we see that the hole behaves like a particle with spin $\frac{3}{2}$, and the second term in Eq. (7) corresponds to the spin-orbit-coupling term. The total angular momentum is $\mathbf{F} = \boldsymbol{L} + \mathbf{J}$. The spin-orbit term couples only hydrogenlike states for which $L = 0, \pm 2$; thus the general forms of the hole wave functions can be written as

$$\Phi(S_{3/2}) = f_0(r)|0,\tfrac{3}{2},\tfrac{3}{2},F_z\rangle + g_0(r)|2,\tfrac{3}{2},\tfrac{3}{2},F_z\rangle , \tag{9a}$$

$$\Phi(P_{1/2}) = f_1(r)|1,\tfrac{3}{2},\tfrac{1}{2},F_z\rangle , \tag{9b}$$

$$\Phi(P_{3/2}) = f_2(r)|1,\tfrac{3}{2},\tfrac{3}{2},F_z\rangle + g_2(r)|3,\tfrac{3}{2},\tfrac{3}{2},F_z\rangle , \tag{9c}$$

$$\Phi(P_{5/2}) = f_3(r)|1,\tfrac{3}{2},\tfrac{5}{2},F_z\rangle + g_3(r)|3,\tfrac{3}{2},\tfrac{5}{2},F_z\rangle , \tag{9d}$$

$$\Phi(D_{5/2}) = f_4(r)|2,\tfrac{3}{2},\tfrac{5}{2},F_z\rangle + g_4(r)|4,\tfrac{3}{2},\tfrac{5}{2},F_z\rangle , \tag{9e}$$

$$\Phi(D_{7/2}) = f_5(r)|2,\tfrac{3}{2},\tfrac{7}{2},F_z\rangle + g_5(r)|4,\tfrac{3}{2},\tfrac{7}{2},F_z\rangle , \tag{9f}$$

where the functions $|L,J,F,F_z\rangle$ are eigenfunctions of the total angular momentum in the L-J coupled scheme and the four figures represent the eigenvalues of the operators $\mathbf{L}$, $\mathbf{J}$, $\mathbf{F}$, and F_z, respectively. The radial functions $f_i(r)$ and $g_i(r)$ can be proved to be solutions of the following set of differential equations:

$$\begin{bmatrix} -(1+C_1)\left[\frac{d^2}{dr^2}+\frac{2}{r}\frac{d}{dr}-\frac{L(L+1)}{r^2}\right]-E & C_2\left[\frac{d^2}{dr^2}+\frac{2L+5}{r}\frac{d}{dr}+\frac{(L+1)(L+3)}{r^2}\right] \\ C_2\left[\frac{d^2}{dr^2}-\frac{2L+1}{r}\frac{d}{dr}+\frac{L(L+2)}{r^2}\right] & -(1-C_1)\left[\frac{d^2}{dr^2}+\frac{2}{r}\frac{d}{dr}-\frac{(L+2)(L+3)}{r^2}\right]-E \end{bmatrix} \begin{bmatrix} f_i(r) \\ g_i(r) \end{bmatrix} = 0 , \tag{10}$$

where the constants C_1 and C_2 for the various states in Eq. (9) are listed in Table I.

To solve Eq. (10) one can expand $f_i(r)$ and $g_i(r)$ in terms of the spherical Bessel functions (3). But for simplicity we would rather use the expansions

$$\begin{aligned} f_i(r) &= \frac{1}{r}\left[\frac{2}{R}\right]^{1/2} \sum_{n=1}^{\infty} a_n \sin\left[\frac{n\pi r}{R}\right] , \\ g_i(r) &= \frac{1}{r}\left[\frac{2}{R}\right]^{1/2} \sum_{n=1}^{\infty} b_n \sin\left[\frac{n\pi r}{R}\right] , \end{aligned} \tag{11}$$

which satisfy the needed boundary conditions; moreover, the corresponding matrix elements of the Hamiltonian can be written as the sine and cosine integrals.[20]

III. ELECTRONIC AND HOLE ENERGY LEVELS

From Eqs. (1) and (10) we see that the energies of the electronic and hole energy levels are all inversely proportional to the square of the spherical radius. Therefore we shall only discuss the energy levels for a square of radius $R = a_0^*$. The energies of the electronic energy levels are given by the zeros of the spherical Bessel functions,[20]

$$E_{nl} = \rho_{nl}^2 . \tag{12}$$

The energies of the hole energy levels are obtained by solving Eq. (10); the variations of the $S_{3/2}$, $P_{3/2}$, and $D_{5/2}$ energy levels with μ are shown in Figs. 1–3. The $P_{5/2}$ and $D_{7/2}$ energy levels are similar to that of $P_{3/2}$ and $D_{5/2}$, respectively, and hence not shown here. The energies of the $P_{1/2}$ energy level are the same as that of the electronic P state, only the effective mass m^* in the effective Rydberg (6) should be replaced by $1/(\gamma_1 + 2\gamma_2)$.

Froms Figs. 1–3 we see that when μ approaches 1, all the energy levels approach zero, which is associated with the fact that for $\mu = 1$ one valence band (heavy-hole band) becomes flat.[19] In the range of μ from 0 to 1 the interaction between the L state and $L+2$ state composing the hole wave function (9) is obviously seen in the figures,

TABLE I. Coefficients in the hole equation of movement (10).

	$S_{3/2}$	$P_{1/2}$	$P_{3/2}$	$P_{5/2}$	$D_{5/2}$	$D_{7/2}$
C_1	0	μ	$-\frac{4}{5}\mu$	$\frac{1}{5}\mu$	$-\frac{5}{7}\mu$	$\frac{2}{7}\mu$
C_2	μ	0	$\frac{3}{5}\mu$	$\frac{2}{5}\sqrt{6}\mu$	$\frac{2}{7}\sqrt{6}\mu$	$\frac{3}{7}\sqrt{5}\mu$

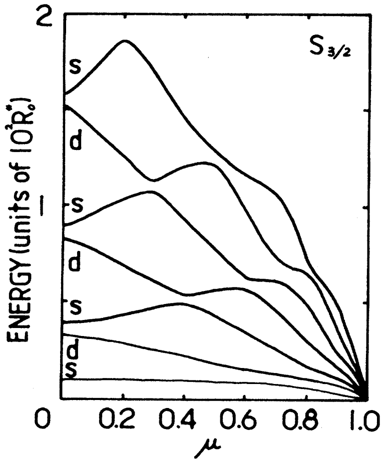

FIG. 1. Hole energy spectrum of the $S_{3/2}$ states as a function of μ.

with the result that the variation of the energy levels with μ is not monotonic. The energy of the $S_{3/2}$ ground state, especially, is nearly a constant over a large range of μ. The result of the $P_{1/2}$ states is not shown in the figure, which energy levels vary according to the linear relation $1+\mu$ and therefore do not approach zero when μ approaches 1. It is associated with the other valence band (light-hole band), which remains parabolic for $\mu=1$.

From the above results it is remarked that if we had not taken into account the mixing of the heavy and light holes, but used the simple parabolic band model, the calculated hole energy levels would vary according to $1+\mu$ and $1-\mu$, respectively, which is clearly not correct.

IV. DONOR AND ACCEPTOR ENERGY LEVELS

Assume that the impurity is located at the center of the sphere. Since the impurity center carries electric charge, the dielectric polarization energy produced by the dielectric small sphere must be taken into account in the calculation of the impurity energy levels. If two charges of magnitude e exist at positions $\mathbf{r}_1$ and $\mathbf{r}_2$ inside the sphere the additional polarization energy is[15]

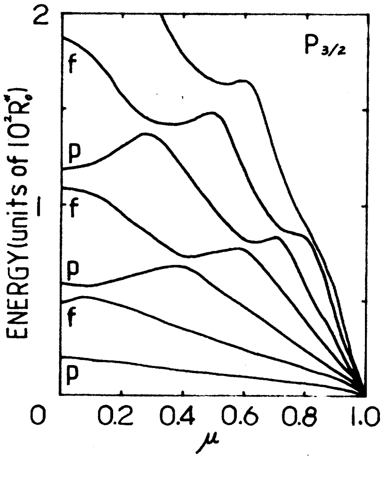

FIG. 2. Hole energy spectrum of the $P_{3/2}$ states as a function of μ.

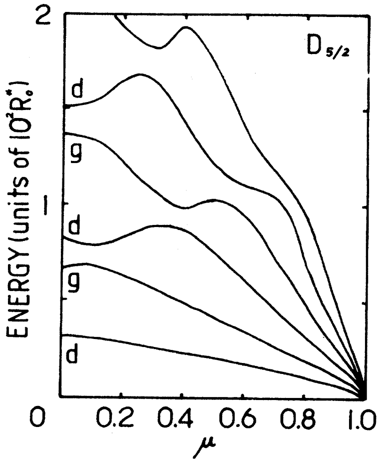

FIG. 3. Hole energy spectrum of the $D_{5/2}$ states as a function of μ.

$$V_p(\mathbf{r}_1,\mathbf{r}_2)=P(r_1)+P(r_2)\pm P_M(\mathbf{r}_1,\mathbf{r}_2)\ , \tag{13}$$

where

$$P(r)=\sum_{n=0}^{\infty}\alpha_n\left[\frac{r}{R}\right]^{2n}\frac{e^2}{2R}\ , \tag{14}$$

$$\alpha_n=\frac{(\epsilon_0-1)(n+1)}{\epsilon_0(\epsilon_0 n+n+1)}\ , \tag{15}$$

$$P_M(\mathbf{r}_1,\mathbf{r}_2)=\sum_{n=0}^{\infty}\alpha_n\frac{e^2 r_1^n r_2^n}{R^{2n+1}}P_n(\cos\theta)\ . \tag{16}$$

P_n is a Legendre polynomial and θ is the angle between $\mathbf{r}_1$ and $\mathbf{r}_2$. The minus and plus signs before P_M in Eq. (13) correspond to opposite and same electric charges, respectively.

For an impurity located at the center $\mathbf{r}_1=0$, $P(r_1)$ and $P_M(\mathbf{r}_1,\mathbf{r}_2)$ are all zero except the $n=0$ term. The $n=0$ term in $P(r_1)$, $P(r_2)$, and $P_M(\mathbf{r}_1,\mathbf{r}_2)$ cancel each other. As a result the polarization energy in the impurity problem is

$$V_p(r)=\sum_{n=1}^{\infty}\alpha_n\left[\frac{r}{R}\right]^{2n}\frac{e^2}{R}\ , \tag{17}$$

where r is the radial coordinate of the electron or hole.

Figure 4 is the variation of the donor s state energies with the sphere radius R. For clarity the ordinate is taken as the energy E multiplied by the square of the radius. Then when R approaches zero the limiting value of ER^2 does not diverge, and the values of ER^2 at $R=0$ are just the eigenenergies without the impurity. The dashed and solid lines are the results without and with the polarization energy included, respectively. From the figure we see that unlike in the bulk material where the impurity produces a series of binding states below the band bottom, in the small semiconductor sphere the impurity only

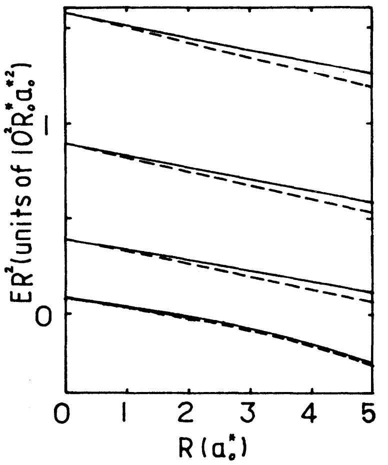

FIG. 4. Energies of the s donor states E multiplied by the squared R as functions of the radius R.

lowers the energies of eigenstates. This is due to the fact that when the crystalline size becomes comparable with a_0^*, the distinction between the impurity states and eigenstates disappears.[11] In the range of R smaller than $5a_0^*$, for all the excited states ER^2 decreases with R linearly, that means that the binding energy (the energy of the impurity state minus that of the eigenstate) decreases with $1/R$. For the ground state ER^2 decreases with R linearly at the beginning; when $R>2a_0^*$, the energy becomes smaller than zero and approaches $-R_0^*$, the limiting value in the bulk material, with ER^2 decreasing parabolically.

The variation of the acceptor $S_{3/2}$ state energies with R for $\mu=0.7$ is shown in Fig. 5. The results are similar to those of donor states, however, the parabolic form of the ER^2 decrease is more obvious for the ground and first excited states. This means that the acceptor states approach the bulk limit at a smaller radius. The cases of other p and d donor states and $P_{3/2}$, $P_{5/2}$, $D_{5/2}$, and $D_{7/2}$ acceptor states are similar to the excited states of the s donor and $S_{3/2}$ acceptor states, respectively: ER^2 decreases with R linearly for $R<5a_0^*$. These results are not shown here.

Figure 6 is the variation of binding energies of the acceptor ground states with μ for $R=a_0^*$. At $\mu=0$, the binding energies of the S, P, and D states become 4.5, 11, and 18 times those in the bulk material, respectively (the donor states are the same). In the range of μ from 0 to 0.9 the binding energies do not change much: that of the $S_{3/2}$ state increases with increase of μ, those of the $P_{3/2}$,$D_{5/2}$ states decrease, and those of the $P_{5/2}$,$D_{7/2}$ states first increase, then decrease. When μ is greater than 0.9 and approaches 1, the binding energies of these states all rise to high values ($10R_0^*-30R_0^*$). There is one exception: the $P_{1/2}$ state, the binding energy of which is basically a constant independent of μ. These results are similar to the acceptor states in the bulk material. The $S_{3/2}$ state, etc., are associated with the heavy-hole band, which becomes flat as $\mu=1$, and the $P_{1/2}$ state is associated with the light-hole band, which is still parabolic as $\mu=1$.

V. OPTICAL TRANSITION PROBABILITY

First, we ignore the exciton effect and calculate the optical transition probability between the conduction- and valence-band states. The hole wave functions are given by Eq. (9), where

$$|L\tfrac{3}{2}FF_z\rangle=\sum_{M_1,M_2}|LM_1\rangle|\tfrac{3}{2}M_2\rangle(LM_1\tfrac{3}{2}M_2|L\tfrac{3}{2}FF_z)\ . \qquad (18)$$

$|LM_1\rangle$ are the angular wave functions, and $|\frac{3}{2}M\rangle$ are the spin -$\frac{3}{2}$ Bloch wave functions at the valence-band top. $(LM_1\frac{3}{2}M_2|L\frac{3}{2}FF_z)$ is the vector-coupling coefficient.[22]

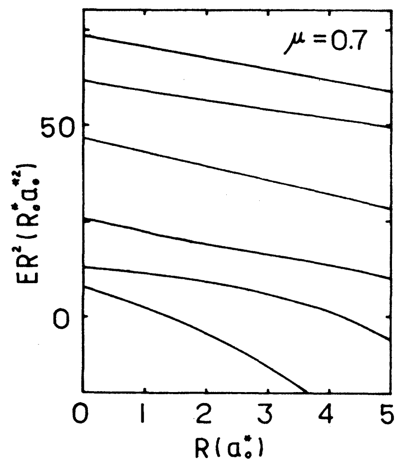

FIG. 5. Energies of the $S_{3/2}$ acceptor states E multiplied by the squared R as functions of the radius R for $\mu=0.7$.

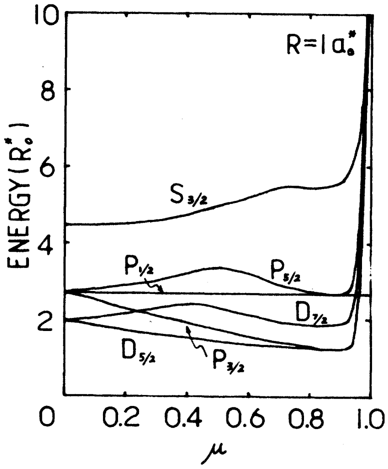

FIG. 6. Binding energies of the acceptor ground states as functions of μ for $R=a_0^*$.

TABLE II. Squared angular parts of the optical-transition-matrix elements $A=|\langle lm|p|FF_z\rangle|^2$ in units of P^2.

Transition	l	m	F	F_z	A	Transition	l	m	F	F_z	A
s-$S_{3/2}$ p_z	0	0	$\frac{3}{2}$	$\frac{1}{2}$	$\frac{2}{3}$	p-$P_{5/2}$ p_z	1	1	$\frac{5}{2}$	$\frac{3}{2}$	$\frac{2}{5}$
p_x	0	0	$\frac{3}{2}$	$\frac{3}{2}$	$\frac{1}{2}$		1	0	$\frac{5}{2}$	$\frac{1}{2}$	$\frac{2}{5}$
	0	0	$\frac{3}{2}$	$-\frac{1}{2}$	$\frac{1}{6}$		1	-1	$\frac{5}{2}$	$-\frac{1}{2}$	$\frac{1}{5}$
p-$P_{1/2}$ p_z	1	0	$\frac{1}{2}$	$\frac{1}{2}$	$\frac{2}{9}$	p_x	1	1	$\frac{5}{2}$	$\frac{5}{2}$	$\frac{1}{2}$
	1	-1	$\frac{1}{2}$	$-\frac{1}{2}$	$\frac{1}{9}$		1	0	$\frac{5}{2}$	$\frac{3}{2}$	$\frac{1}{5}$
p_x	1	-1	$\frac{1}{2}$	$\frac{1}{2}$	$\frac{1}{4}$		1	-1	$\frac{5}{2}$	$\frac{1}{2}$	$\frac{1}{20}$
	1	1	$\frac{1}{2}$	$\frac{1}{2}$	$\frac{1}{36}$		1	1	$\frac{5}{2}$	$\frac{1}{2}$	$\frac{1}{20}$
	1	0	$\frac{1}{2}$	$-\frac{1}{2}$	$\frac{1}{18}$		1	0	$\frac{5}{2}$	$-\frac{1}{2}$	$\frac{1}{10}$
p-$P_{3/2}$ p_z	1	1	$\frac{3}{2}$	$\frac{3}{2}$	$\frac{4}{15}$		1	-1	$\frac{5}{2}$	$-\frac{3}{2}$	$\frac{1}{10}$
	1	0	$\frac{3}{2}$	$\frac{1}{2}$	$\frac{2}{45}$	d-$D_{3/2}$ p_z	2	1	$\frac{3}{2}$	$\frac{3}{2}$	$\frac{4}{15}$
	1	-1	$\frac{3}{2}$	$-\frac{1}{2}$	$\frac{16}{45}$		2	0	$\frac{3}{2}$	$\frac{1}{2}$	$\frac{2}{15}$
p_x	1	0	$\frac{3}{2}$	$\frac{3}{2}$	$\frac{3}{10}$		2	-2	$\frac{3}{2}$	$-\frac{3}{2}$	$\frac{4}{15}$
	1	-1	$\frac{3}{2}$	$\frac{1}{2}$	$\frac{1}{5}$	p_x	2	0	$\frac{3}{2}$	$\frac{3}{2}$	$\frac{1}{10}$
	1	1	$\frac{3}{2}$	$\frac{1}{2}$	$\frac{4}{45}$		2	-1	$\frac{3}{2}$	$\frac{1}{2}$	$\frac{1}{5}$
	1	0	$\frac{3}{2}$	$-\frac{1}{2}$	$\frac{1}{90}$		2	-2	$\frac{3}{2}$	$-\frac{1}{2}$	$\frac{1}{5}$
	1	-1	$\frac{3}{2}$	$-\frac{3}{2}$	$\frac{1}{15}$		2	2	$\frac{3}{2}$	$\frac{3}{2}$	$\frac{1}{15}$
							2	0	$\frac{3}{2}$	$-\frac{1}{2}$	$\frac{1}{30}$
							2	-1	$\frac{3}{2}$	$-\frac{3}{2}$	$\frac{1}{15}$

The electronic wave function is given by

$$\Phi_e=f_e(r)|lm\rangle|S\sigma\rangle \ , \tag{19}$$

where $f_e(r)|lm\rangle$ is the orbital wave function, $|S\sigma\rangle$ is the Bloch wave function at the conduction-band bottom, and σ is the spin component. Thus the optical-transition-matrix element

$$\langle\Phi_e|\mathbf{p}|\Phi_n\rangle=\int dr\, r^2 f_e(r)f_h(r) \times\sum_{M_1,M_2}\langle lm|LM_1\rangle\langle S\sigma|\mathbf{p}|\tfrac{3}{2}M_2\rangle \times(LM_1\tfrac{3}{2}M_2|L\tfrac{3}{2}FF_z) \ . \tag{20}$$

Because of the orthonormality of angular momentum eigenfunctions $\langle lm|LM_1\rangle=\delta_{lL}\delta_{mM_1}$, there is only one term in the hole wave function (9) contributing to the matrix element (20). We call the first part in Eq. (20) the overlap integral and the second part the angular part of the transition-matrix element

$$\langle lm|\mathbf{p}|FF_z\rangle=\sum_{M_2}\langle S\sigma|\mathbf{p}|\tfrac{3}{2}M_2\rangle(lm\tfrac{3}{2}M_2|l\tfrac{3}{2}FF_z) \ . \tag{21}$$

Table II gives the values of $|\langle lm|\mathbf{p}|FF_z\rangle|^2$ calculated from Eq. (21), in units of $P^2=|\langle S|p_x|X\rangle|^2$, where S and X are the Bloch wave functions of the conduction-band bottom and valence-band top, respectively. In Table II we have the transition selection rules from the $|lm\rangle$ state to the $|FF_z\rangle$ state. For simplicity we only list the results of the $|S\uparrow\rangle$ state; the results of $|S\downarrow\rangle$ state are the same but the signs of F_z reverse. The results of the p_y transition are the same as that of the p_x transition; only the p_x

TABLE III. Overlap integrals of the radial wave functions in various possible transitions for hole parameter $\mu=0.7$.

s-S	p-P	p-P	d-S	d-D
1-1 0.833	1-1 0.987	1-1 0.574	1-1 0.439	1-1 0.954
1-2 0.543	2-2 0.934	1-2 0.746	1-1 0.602	1-2 0.267
2-1 0.333	2-5 0.308	1-3 0.318	2-3 0.713	2-2 0.890
2-2 0.577	3-3 0.940	2-1 0.431	2-9 0.556	2-6 0.376
3-3 0.680	3-9 0.322	2-2 0.403	3-4 0.704	3-3 0.910
3-8 0.414	4-4 0.939	2-5 0.331	4-6 0.700	3-9 0.291
3-9 0.588	5-5 0.364	3-3 0.571	5-7 0.708	4-4 0.913
4-4 0.683	5-6 0.873	3-9 0.765		5-5 0.881
5-6 0.690		4-4 0.604		5-6 0.266

TABLE IV. Binding energies of the lowest three $(s,S_{3/2})$ exciton states as functions of R. The second rows are the results without including the polarization energies. The energies are in units of meV, the R are in units of Å.

R	40	80	120	160	200
(1-1)	36.94	18.92	12.93	9.93	8.14
	55.00	27.66	18.55	14.00	11.28
(1-2)	16.00	8.90	6.50	5.28	4.48
	44.27	22.27	14.94	11.28	9.08
(1-3)	18.20	8.28	5.00	3.39	2.46
	49.53	24.65	16.36	12.20	9.71

transition results are listed. Because of the spherical symmetry, although the individual transition probability and selection rule are different for the p_z and p_x transitions, the summation of the transition probabilities of all the possible transitions is equal and independent of the electric polarization direction.

The overlap integrals of the radial wave functions in Eq. (20) for the possible transitions in the case of $\mu=0.7$ are listed in Table III. Since the hole equation (10) couples the orbital wave functions with different L and n, the optical transitions do not follow the selection rule $\Delta n=0$ strictly. For example, for the s-$S_{3/2}$ transition the electronic $n=1$ level can make the transition to both hole $n=1$ and $n=2$ levels, and besides the electronic s state, the electronic d state can also make the transition to the hole $S_{3/2}$ state.

VI. EXCITON STATES

If we take the electronic effective Bohr radius a_0^* and effective Rydberg R_0^* as units of length and energy, the exciton Hamiltonian is

$$H=p_e^2+m_e^*\gamma_1\left[p_h^2-\frac{\mu}{9}(P_h^{(2)}\cdot J^{(2)})\right]-\frac{2}{r_{eh}}+V_p(\mathbf{r}_e,\mathbf{r}_h)\ . \tag{22}$$

The exciton wave function can be written as

$$\Phi_{\text{ex}}=\sum_{i,j}c_{ij}\Phi_{ei}(\mathbf{r}_e)\Phi_{hj}(\mathbf{r}_h)\ , \tag{23}$$

where $\Phi_{ei}(\mathbf{r}_e)$ and $\Phi_{hj}(\mathbf{r}_h)$ are the wave functions of electronic and hole eigenstates, respectively. Putting the wave function (23) in the Schrödinger equation, we obtain the secular equation,

$$|H_{ij,i'j'}-E\delta_{ii'}\delta_{jj'}|=0\ , \tag{24}$$

where the Hamiltonian matrix elements

$$\begin{aligned}
H_{ij,i'j'}&=(H_0)_{ij,i'j'}+(H_1)_{ij,i'j'}\ ,\\
(H_0)_{ij,i'j'}&=(E_{ei}+m_e^*\gamma_1E_{nj})\delta_{ii'}\delta_{jj'}\ ,\\
(H_1)_{ij,i'j'}&=\left[-\frac{2}{r_{eh}}+V_p(\mathbf{r}_e,\mathbf{r}_h)\right]_{ij,i'j'}\ .
\end{aligned} \tag{25}$$

The integration of the Coulomb interaction is calculated by using[22]

$$\frac{1}{r_{12}}=\sum_{k=0}^{\infty}V_k(r_1,r_2)P_k(\cos\theta),\quad V_k(r_1,r_2)=\frac{r_<^k}{r_>^{k+1}} \tag{26}$$

where P_k are the Legendre polynomials, θ is the angle between $\mathbf{r}_1$ and $\mathbf{r}_2$, and $r_<$ is the lesser and $r_>$ the greater of r_1 and r_2. By use of the theory of angular momentum coupling[22] it can be proven that

$$\begin{aligned}
&\left\langle\Phi_{\text{ex}}(s,S_{3/2})\left|\frac{1}{r_{eh}}\right|\Phi'_{\text{ex}}(s,S_{3/2})\right\rangle\\
&\quad=\overline{V_0(r_e,r_h)}|_{f_sf_0}+\overline{V_0(r_e,r_h)}|_{f_sg_0}+\tfrac{1}{25}\overline{V_2(r_e,r_h)}|_{f_sg_0}\ ,
\end{aligned} \tag{27}$$

$$\left\langle\Phi_{\text{ex}}(p,P_{1/2})\left|\frac{1}{r_{eh}}\right|\Phi'_{\text{ex}}(p,P_{1/2})\right\rangle=\overline{V_0(r_e,r_h)}|_{f_pf_1}\ , \tag{28}$$

TABLE V. Binding energies of the lowest three $(p,P_{1/2})$ exciton states as functions of R. The energies are in units of meV, the R are in units of Å.

R	40	80	120	160	200
(1-1)	13.56	7.02	4.84	3.75	3.09
	43.87	21.97	14.66	11.01	8.82
(1-2)	12.15	6.23	4.26	3.28	2.69
	44.75	22.44	14.99	11.28	9.05
(2-1)	12.10	6.17	4.20	3.20	2.62
	44.63	22.31	14.87	11.15	8.92

TABLE VI. Energy band parameters of ZnSe and GaAs, m_e^*, m_h^*, m_l^*, and m_Δ^* are effective masses of the electron, heavy hole, light hole, and hole of the split-off band (in units of m_0); Δ is the spin-orbit splitting energy of the valence band (in units of eV).

	m_e^*	m_h^*	m_l^*	m_Δ^*	γ_1	γ_2	Δ	ϵ_0
ZnSe	0.160	0.780	0.145	0.200	4.089	1.404	0.430	8.300
GaAs	0.067	0.475	0.087	0.133	6.800	2.347	0.340	12.530

where

$$\overline{V_0(r_e,r_h)}|_{f_sf_0}=\int\int f_s(r_e)f_0(r_h)V_0(r_e,r_h)$$
$$\times f_s'(r_e)f_0'(r_h)r_e^2dr_er_h^2dr_h\ , \qquad (29)$$

etc. Equations (27)–(29) are equally applicable to calculation of the matrix elements of the polarization potential $p_M(\mathbf{r}_e,\mathbf{r}_h)$ [Eq. (16)].

We calculated the exciton binding energies (the exciton energy minus the energies of corresponding electronic and hole eigenstates) in the GaAs small spheres; the energy band parameters are given in Table VI. The binding energies of the $(s,S_{3/2})$ and $(p,P_{1/2})$ excitons as functions of R are given in Tables IV and V, respectively, where the second rows are the results without including the polarization energy. The dielectric polarization of the small sphere decreases the exciton binding energies, especially for the case of small radius. The binding energies increase rapidly with decrease of R; that of the $(s,S_{3/2})$ ground-state exciton increases most obviously, reaching 37 meV at $R=40$ Å. The binding energies decrease with increase of the excited-state energies.

VII. ENERGY LEVELS OF ZnSe CRYSTALLINE SPHERES

As an illustration of the above calculation results we consider the energy levels of the ZnSe crystalline spheres. ZnSe has a zinc-blende structure and a larger spin-orbit splitting in the valence bands; furthermore, it has been investigated experimentally.[12] In Table VI we give the energy band parameters of ZnSe and GaAs (Ref. 23) used in this paper. It is noticed that the band parameter μ [Eq. (8)] for ZnSe and GaAs are nearly 0.7, so that the results in Secs. IV and V (Fig. 5 and Table III) are applicable to these two materials.

From Eq. (12) and Figs. 1–3 we obtain the energy levels of the ZnSe crystalline sphere as functions of the radius R, as shown in Fig. 7. For clarity only the $S_{3/2}$ series of the hole energy levels are shown; the dashed lines are the hole 1s energy level and the top of the split-off band, respectively. Chestnoy *et al.*[12] observed and analyzed, for the first time, the second excited electronic state of $R\simeq 20$-Å ZnS and ZnSe clusters. They assigned the two resolved transitions to the $1S(\Gamma_8)$ and $1S(\Gamma_7)$ transitions. From Fig. 7 we see that this is the only possible explanation, because the splitting of the two transition peaks, i.e. the difference between the first $S_{3/2}$ hole energy level and the 1s split-off hole energy level, slightly increases with decreasing ZnSe cluster size. In Table VII we give the calculated energies of the electronic 1s, hole $1S_{3/2}$, and split-off 1s states at some values of the sphere radius, plus the energy gap 2.58 eV; we obtain the transition energies as functions of R, compared with the experimental values.[12]

From Table VII we see that the small sphere (ZnSe, A or B in Ref. 12) corresponds to a radius $R=17$ Å, and the moderate one (ZnSe, C) corresponds to $R=25$ Å (shown by arrows in Fig. 7). It should be indicated that there is no experimental value of the split-off hole effective mass m_Δ^*; the $m_\Delta^*=0.2m_0$ in Table VI is fitted from this experiment. If m_Δ^* is larger than $0.2m_0$, the splitting of the two transitions will be smaller; if m_Δ^* is larger than $0.2m_0$, the splitting will be larger. Therefore, by comparison of the experimental and theoretical results we obtained the radii of the spheres, and in the meantime the split-off hole effective mass. Besides the 1s-$1S_{3/2}$ transition, there can also be a 1s-$2S_{3/2}$ transition due to the S-D mixing. In the case of $\mu=0$ there is no S-D coupling, the first state is an s state, and the second one is a d state, as shown in Fig. 1. At $\mu=0.7$, there is stronger S-D coupling, from Table III we see that the overlap integrals of the radial wave functions are 0.833 and 0.543 for the 1s-$1S_{3/2}$ and 1s-$2S_{3/2}$ transitions, respectively. Thus the transition probability of the 1s-$1S_{3/2}$ transition is 2.4 times that of the 1s-$2S_{3/2}$ transition. Because the

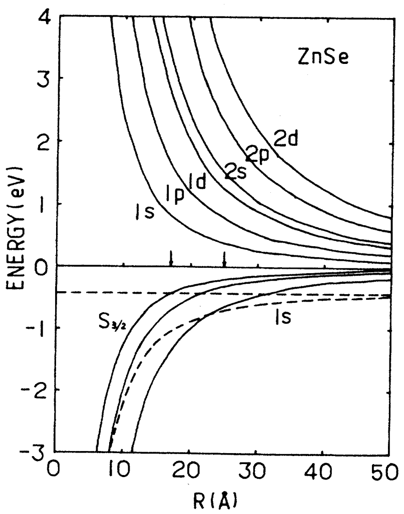

FIG. 7. Energies of electronic and hole states of ZnSe spheres as functions of radius R. The dashed lines are for the split-off valence band.

TABLE VII. Calculated energies of the electronic 1s, hole 1$S_{3/2}$, and split-off hole 1s states of ZnSe spheres for some radii (relative to the conduction-band bottom and the valence-band top, respectively) and corresponding transition energies. Experimental transition energies are also given (all in units of eV).

R (Å)	16	17	18	Expt.	24	25	26	Expt.
1s	0.918	0.813	0.725		0.408	0.376	0.348	
1$S_{3/2}$	−0.502	−0.445	−0.397		−0.223	−0.206	−0.190	
1s_Δ	−1.164	−1.080	−1.010		−0.756	−0.731	−0.708	
1s-1$S_{3/2}$	4.000	3.838	3.702	3.874	3.211	3.162	3.118	3.179
1s-1s_Δ	4.662	4.473	4.315	4.428	3.744	3.687	3.636	3.647

energy of the hole excited states approaches that of the split-off valence band as the sphere radius decreases, there may be some resonance between the $\Gamma_8 D$ states and the $\Gamma_7 S$ states, which is not considered in our strong spin-orbit coupling approximation.

VIII. SUMMARY

In this paper we studied the electronic structures of spherical ZDS's by the Baldereschi and Lipari[19] spherical-model Hamiltonian in the limit of strong spin-orbit coupling. The mixing effect of the heavy and light holes is taken into account, and the symmetry classification and energies of the hole energy levels are obtained. It is found that the hole energy levels are apparently different from that obtained by the simple-parabolic-band model. When the radius of the crystalline sphere decreases, there appears a series of quantum size effects. The distinction between the shallow impurity state and the eigenstate disappears; the impurity Coulomb potential only causes the lowering of the energies of eigenstates. For $R=a_0^*$ and $\mu=0$, the binding energies of the S, P, and D acceptor (and donor) ground states become about 4.5, 11, and 18 times those in the bulk materials, respectively. They decrease as $1/R$ and approach the limiting values in the bulk materials as R increases. The optical transition probabilities and the selection rules between the conduction and valence states are obtained. Because of the mixing of the L and $L+2$ states in the hole wave functions the $\Delta n=0$ selection rule is not followed strictly. The s and p excitons in the GaAs small sphere are also calculated. The dielectric polarization of the small sphere decreases the exciton binding energies, and this effect is especially obvious in the case of small radius. The exciton binding energy increases rapidly with decrease of R; as $R=40$ Å, the binding energy of the $(s,S_{3/2})$ ground-state exciton reaches 37 meV. The energy levels of the ZnSe crystalline sphere are given as functions of the radius R, and compared with the experiments.

ACKNOWLEDGMENTS

This work was supported by the Chinese National Natural Science Foundation.

---

[1] M. A. Reed, R. T. Bate, K. Bradshaw, W. M. Duncan, W. R. Frensley, J. W. Lee, and H. D. Shih, J. Vac. Technol. B **4**, 358 (1986).

[2] K. Kash, A. Scherer, J. M. Worlock, H. G. Craighead, and M. C. Tamargo, Appl. Phys. Lett. **49**, 1043 (1986).

[3] J. Cibert, P. M. Petroff, G. J. Dolan, S. J. Pearton, A. C. Gossard, and J. H. English, Appl. Phys. Lett. **49**, 1275 (1986).

[4] H. Temkin, G. J. Dolan, M. B. Panish, and S. N. G. Chu, Appl. Phys. Lett. **50**, 413 (1987).

[5] M. A. Reed, J. N. Randall, R. J. Aggarwal, R. J. Matyi, T. M. Moore, and A. E. Wetsel, Phys. Rev. Lett. **60**, 535 (1988).

[6] C. Hayashi, Phys. Today **40**, (12), 44 (1987).

[7] A. Henglein and B. Bunsenges, Phys. Chem. **86**, 301 (1982).

[8] D. Duonghong, J. Ramsden, and M. Gratzel, J. Am. Chem. Soc. **104**, 2977 (1982).

[9] J. Kuczynski and J. K. Thomas, Chem. Phys. Lett. **88**, 445 (1982).

[10] M. A. Fox, B. Lindig, and C. C. Chen, J. Am. Chem. Soc. **104**, 5828 (1982).

[11] L. E. Brus, J. Chem. Phys. **90**, 2555 (1986), and references cited therein.

[12] N. Chestnoy, R. Hull, and L. E. Brus, J. Chem. Phys. **85**, 2237 (1986).

[13] J. B. Xia and K. Huang, Chin. J. Semicond. **8**, 564 (1987); Chin. Phys. (to be published).

[14] J. A. Brum, G. Bastard, L. L. Chang, and L. Esaki, Superlatt. Microstruct. **3**, 47 (1987).

[15] L. E. Brus, J. Chem. Phys. **79**, 5566 (1983); **80**, 4403 (1984).

[16] A. Baldereschi and N. O. Lipari, Phys. Rev. B **3**, 439 (1971).

[17] Y. Kayanuma, Solid State Commun. **59**, 405 (1986).

[18] S. V. Nair, S. Sinha, and K. C. Rustagi, Phys. Rev. B **35**, 4098 (1987).

[19] A. Baldereschi and N. O. Lipari, Phys. Rev. B **8**, 2697 (1973).

[20] *Handbook of Mathematical Functions with Formulas, Graphs and Mathematical Tables,* edited by M. Abramowitz and I. Stegun (U.S. Department of Commerce, National Bureau of Standards, 1964).

[21] J. M. Luttinger, Phys. Rev. **102**, 1030 (1956).

[22] A. R. Edmonds, *Angular Momentum in Quantum Mechanics* (Princeton University Press, Princeton, NJ, 1957).

[23] O. Madelung, M. Schulz, and H. Weiss, *Numerical Data and Functional Relationships in Science and Technology* (Springer-Verlag, Berlin, 1982), Vol. 17.